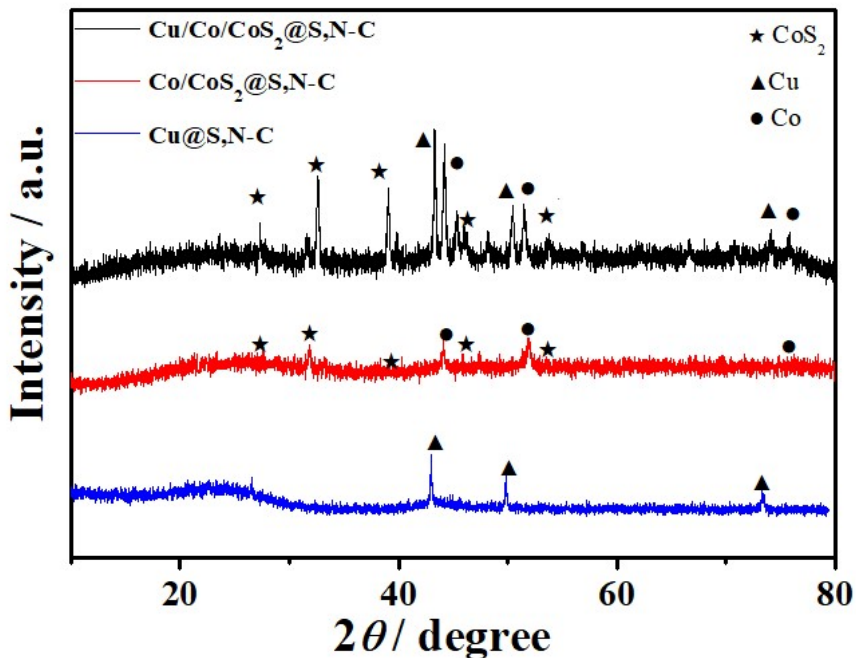
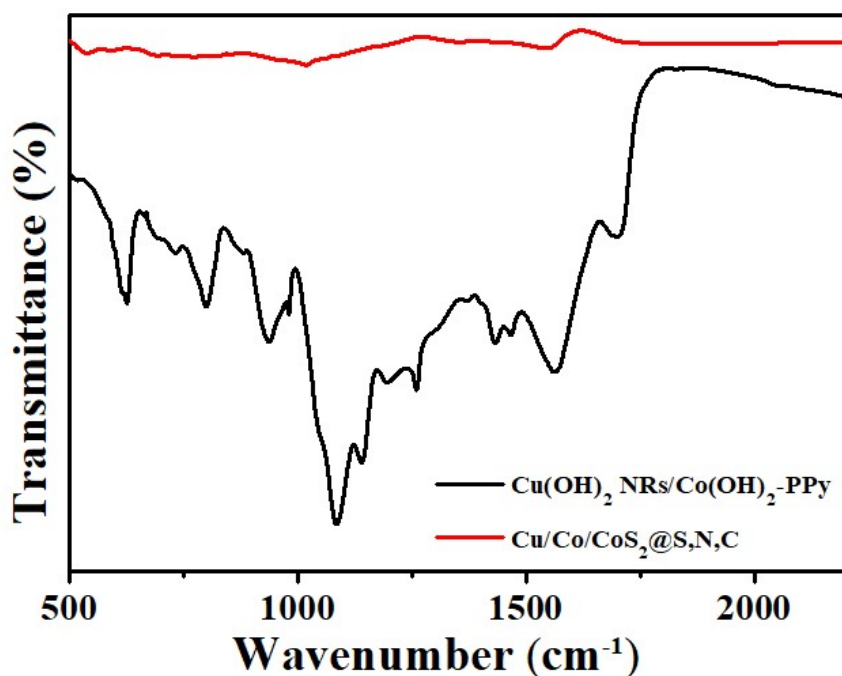


-Electronic Supplementary Information-



**Figure S1.** XRD pattern of as-prepared  $\text{Cu}/\text{Co}/\text{CoS}_2@\text{S,N-C}$ ,  $\text{Co}/\text{CoS}_2@\text{S,N-C}$ ,  $\text{Cu}@\text{S,N-C}$ .



**Figure S2.** FTIR spectra of  $\text{Cu}(\text{OH})_2$  NRs/ $\text{Co}(\text{OH})_2$  NSs-PPy and  $\text{Cu}/\text{Co}/\text{CoS}_2@\text{S,N-C}$ .

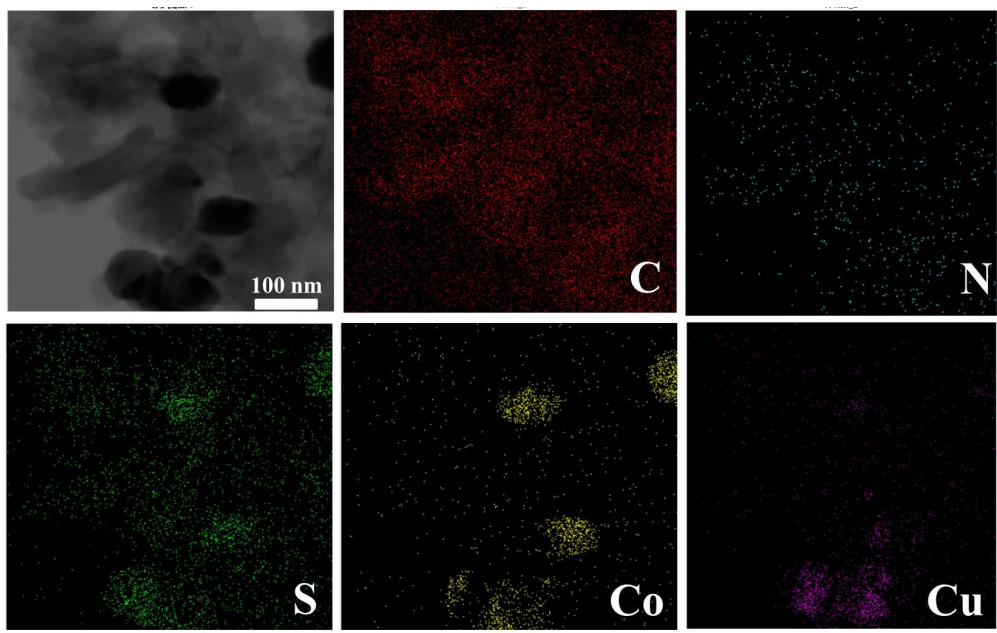


**Figure S3.** The corresponding elemental mapping images for C, N, S, Cu and Co of Cu/Co/CoS<sub>2</sub>@S,N-C.

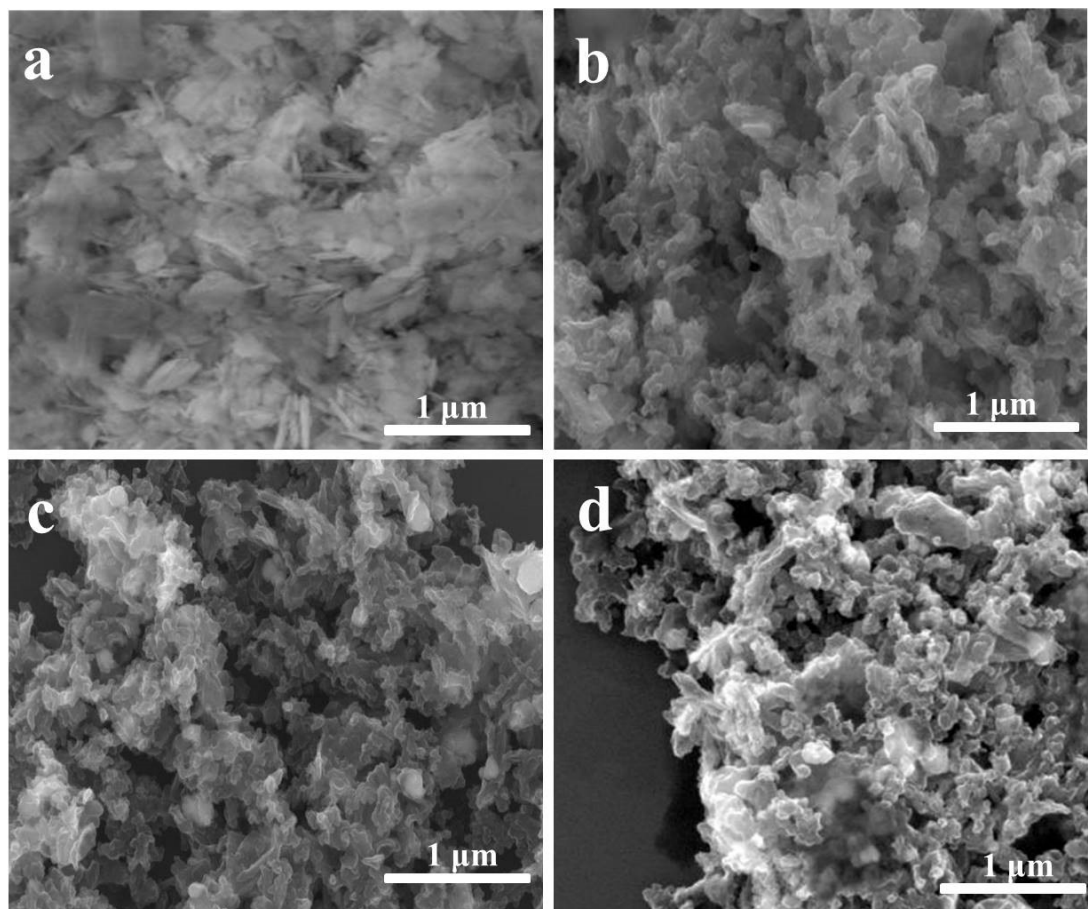


**Figure S4.** SEM images of (a) Cu(OH)<sub>2</sub> NRs/Co(OH)<sub>2</sub> NSs, (b) Cu(OH)<sub>2</sub> NRs/Co(OH)<sub>2</sub> NSs-PPy, (c) Cu/Co/CoS<sub>2</sub>@S,N-C and (d) Cu/Co/CoS<sub>2</sub>@S,N-C after 30000 s.

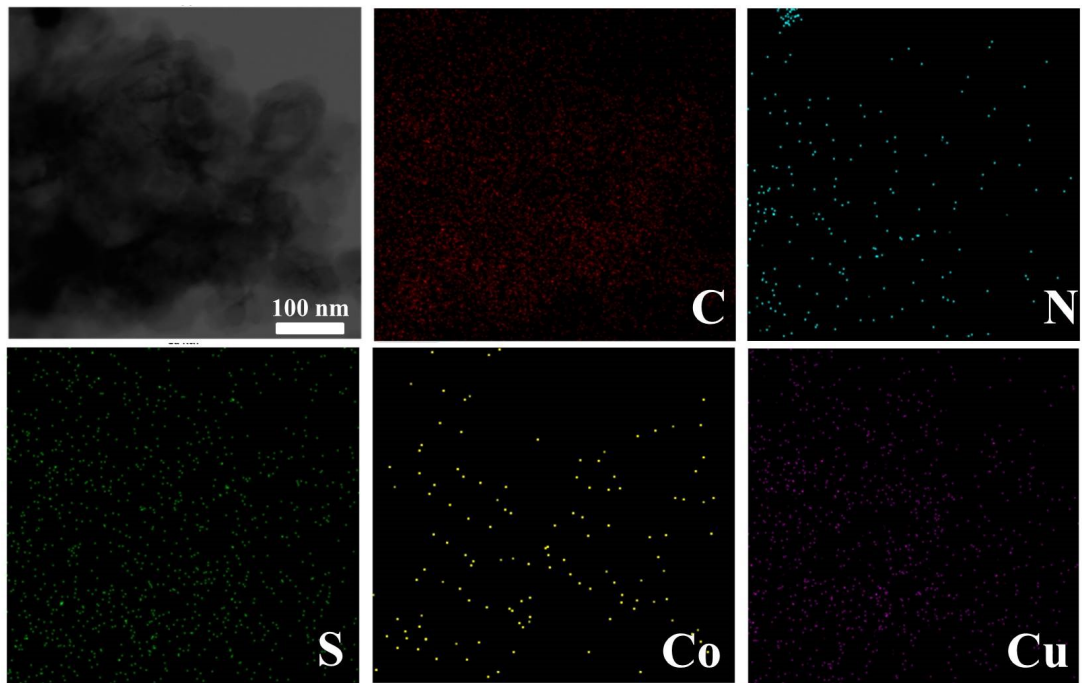


**Figure S5.** The corresponding elemental mapping images for C, N, S, Cu and Co of Cu/Co/CoS<sub>2</sub>@S,N-C after 30000 s.

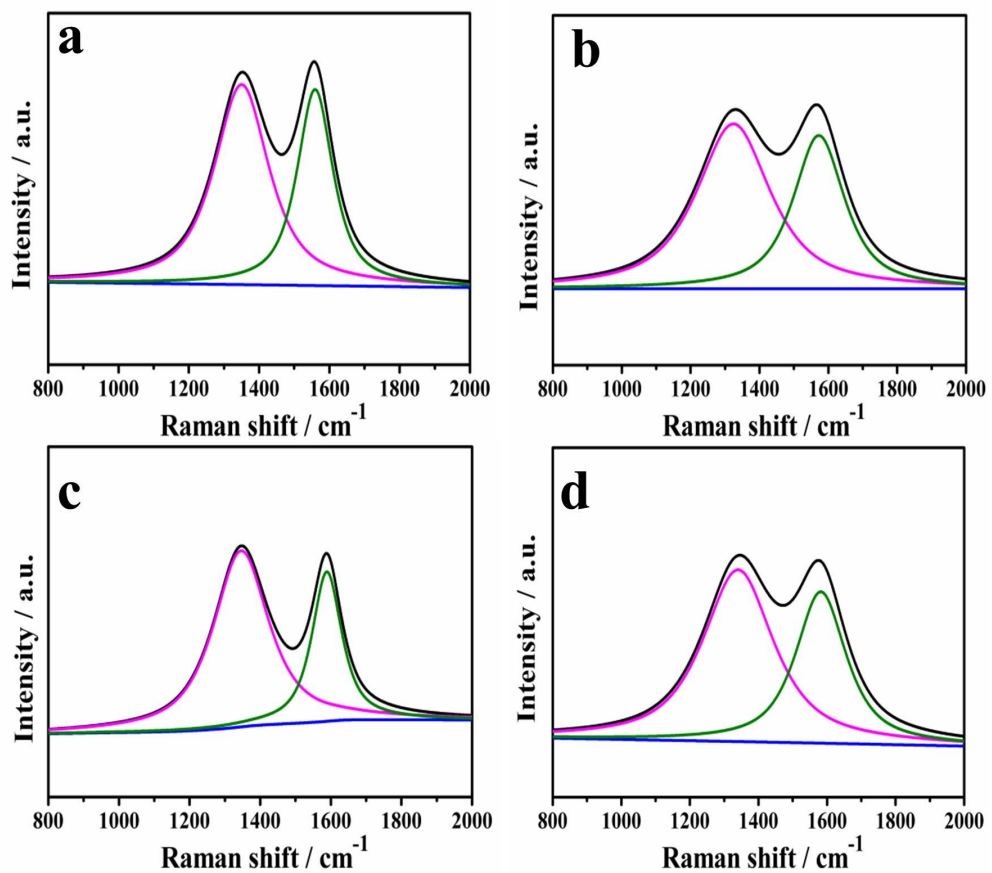


**Figure S6.** Raman spectra of Cu/Co/CoS<sub>2</sub>@S,N-C-900 (a), Cu/Co/CoS<sub>2</sub>@S,N-C-1100 (b), Cu/Co/CoS<sub>2</sub>@S,N-C (1 mg), Cu/Co/CoS<sub>2</sub>@S,N-C (20 mg).

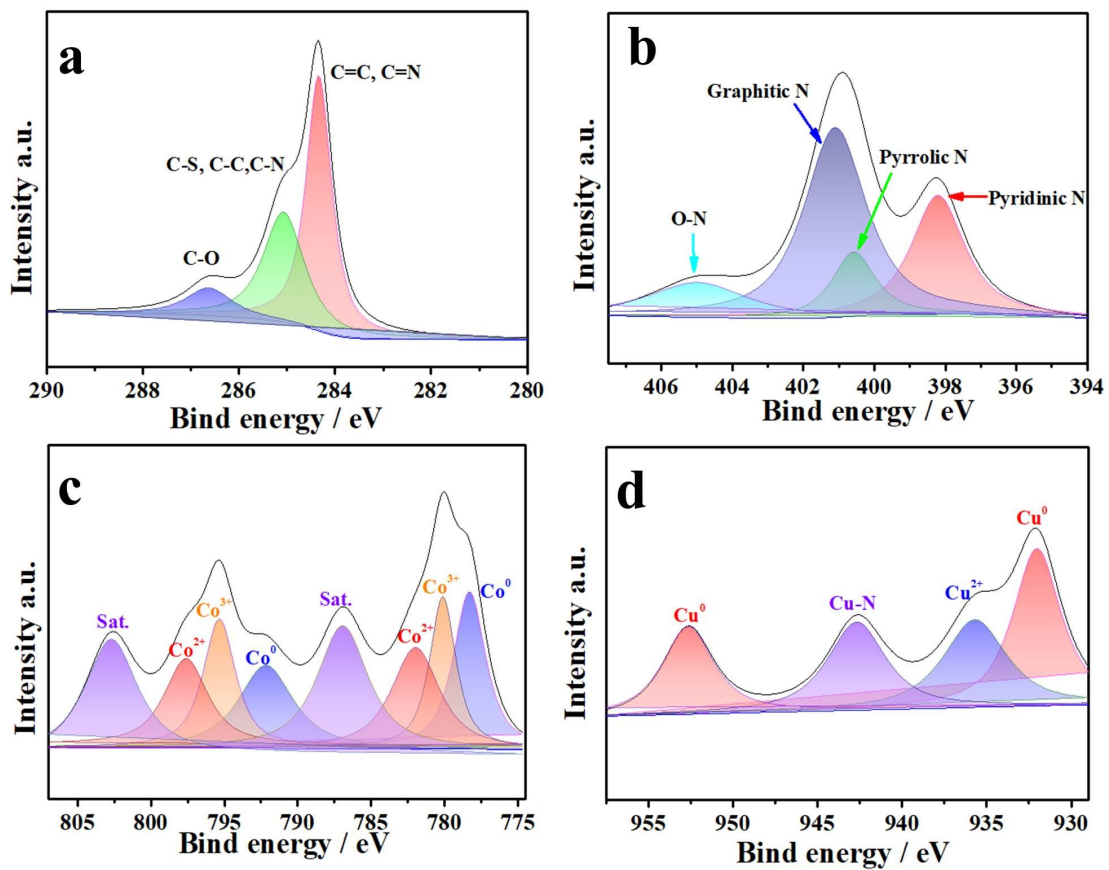


**Figure S7.** High-resolution C 1s (a), N 1s (b), Co 2p (c), Cu 2p (d), spectra of Cu/Co/@NC.

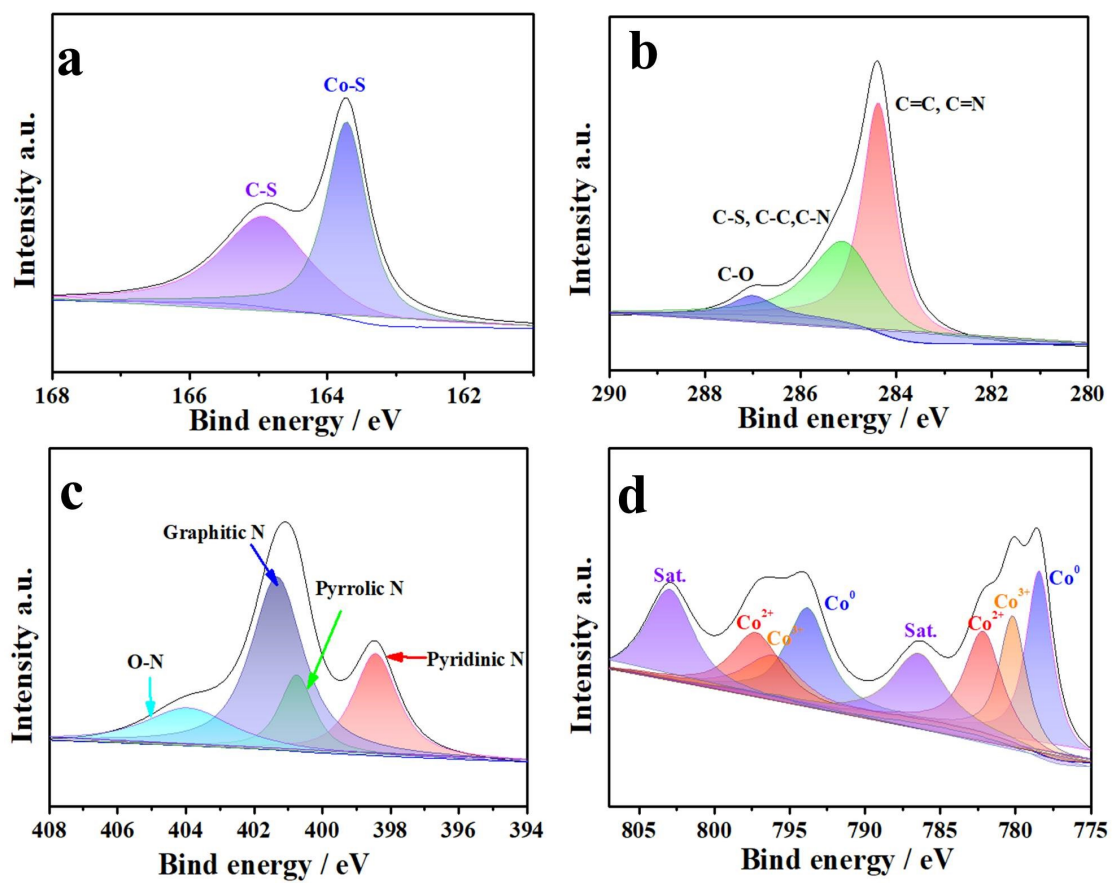


**Figure S8.** High-resolution S 1s (d), C 1s (a), N 1s (b), Co 2p (c), spectra of Co/CoS<sub>2</sub>@S,N-C.

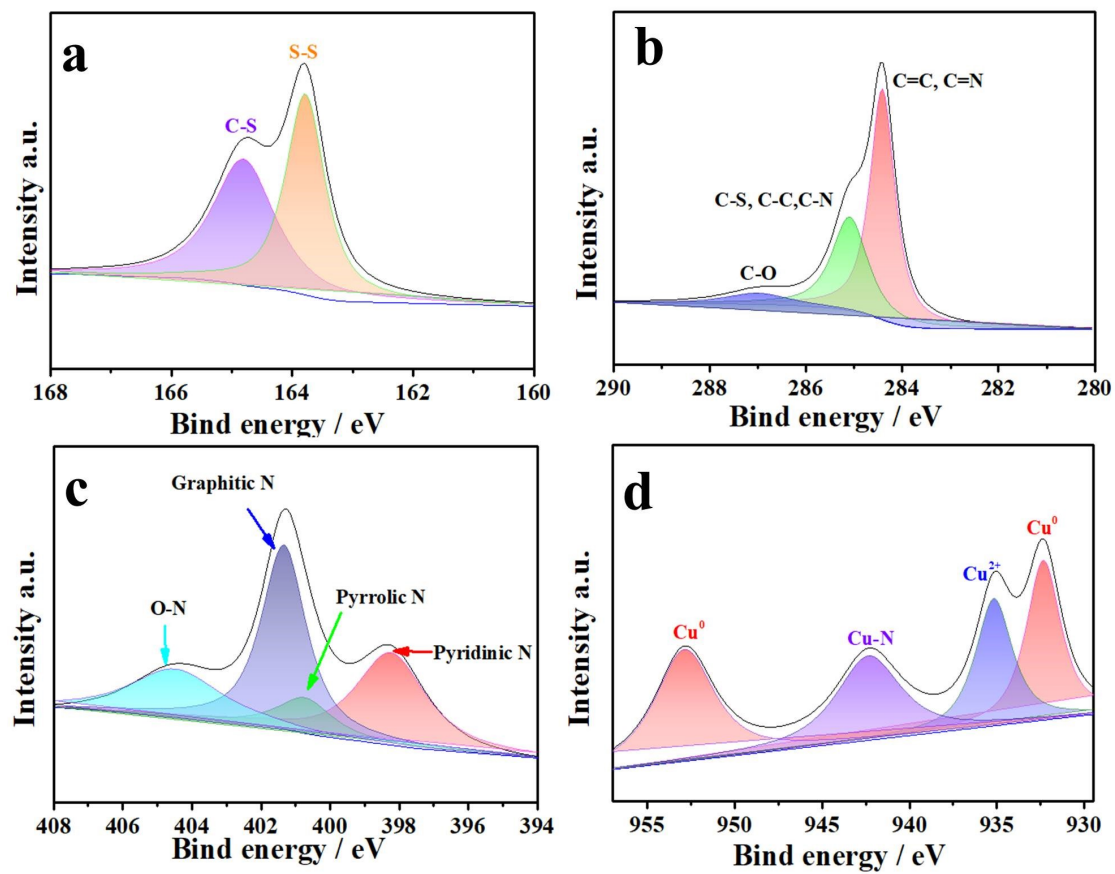


**Figure S9.** High-resolution S 1s (d), C 1s (a), N 1s (b), Co 2p (c), spectra of Cu@S,N-C.

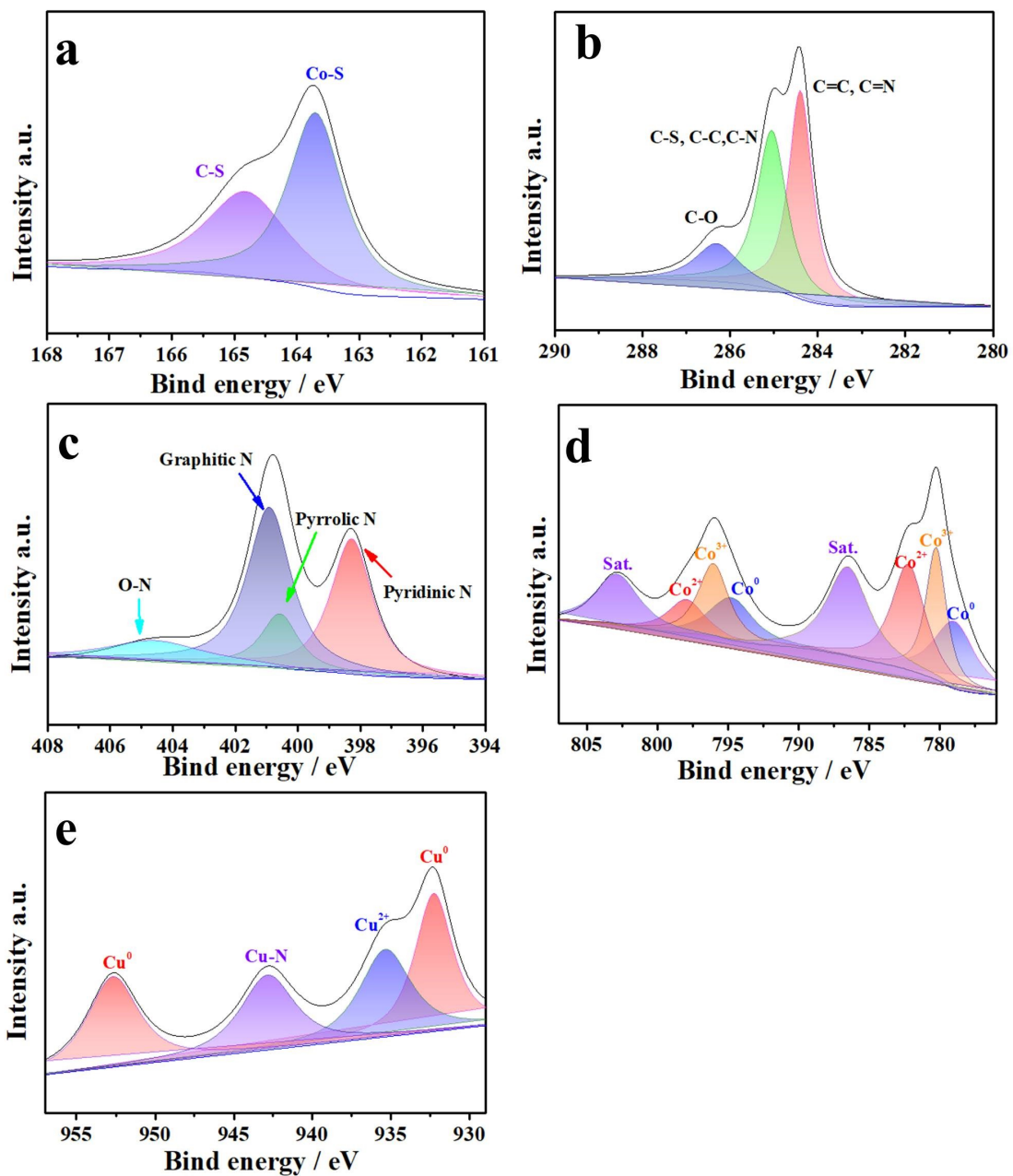


**Figure S10.** High-resolution S 1s (d), C 1s (a), N 1s (b), Co 2p (c), spectra of Cu/Co/CoS<sub>2</sub>@S,N-C-900.

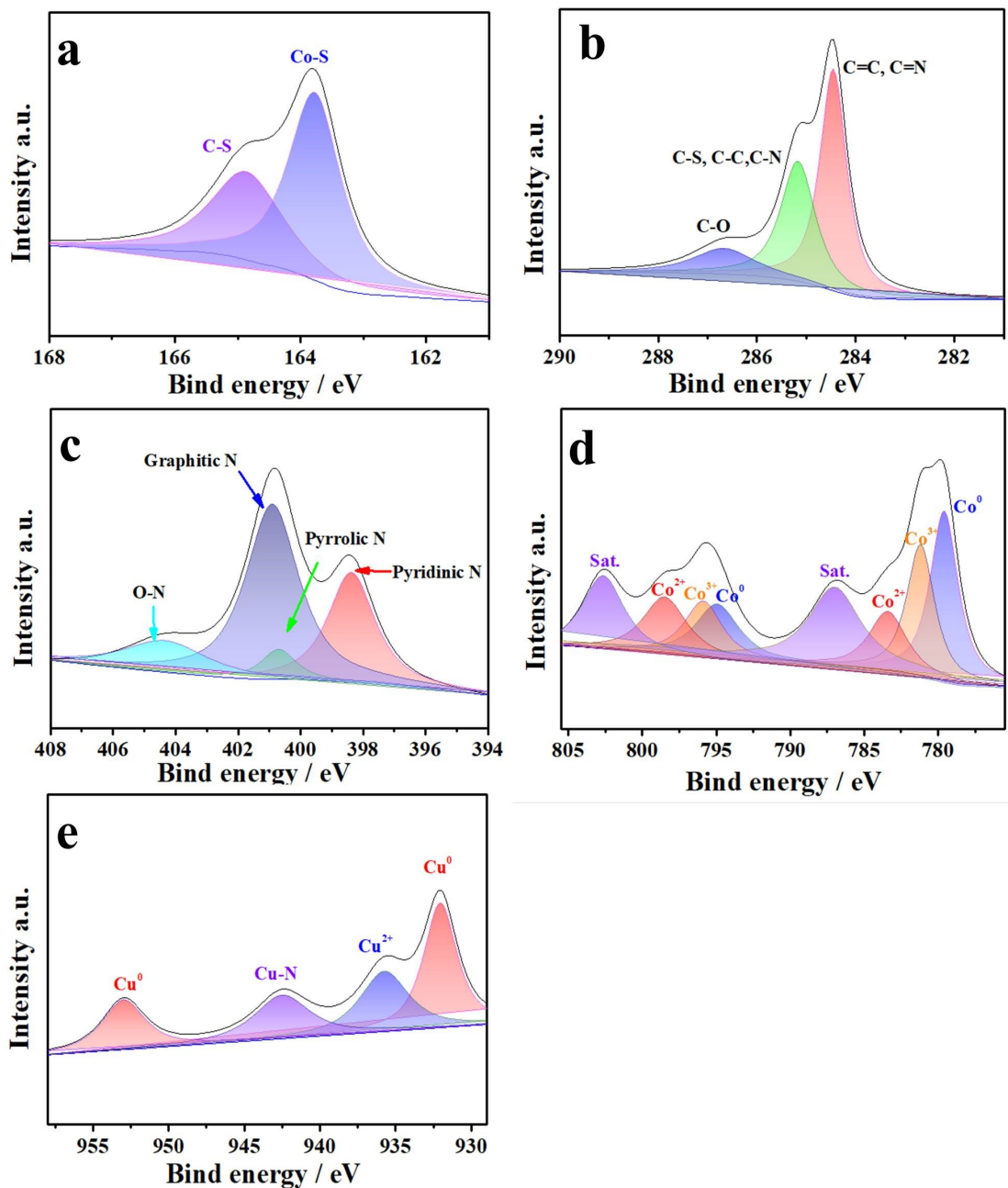


**Figure S11.** High-resolution S 1s (d), C 1s (a), N 1s (b), Co 2p (c), spectra of Cu/Co/CoS<sub>2</sub>@S,N-C-1100.

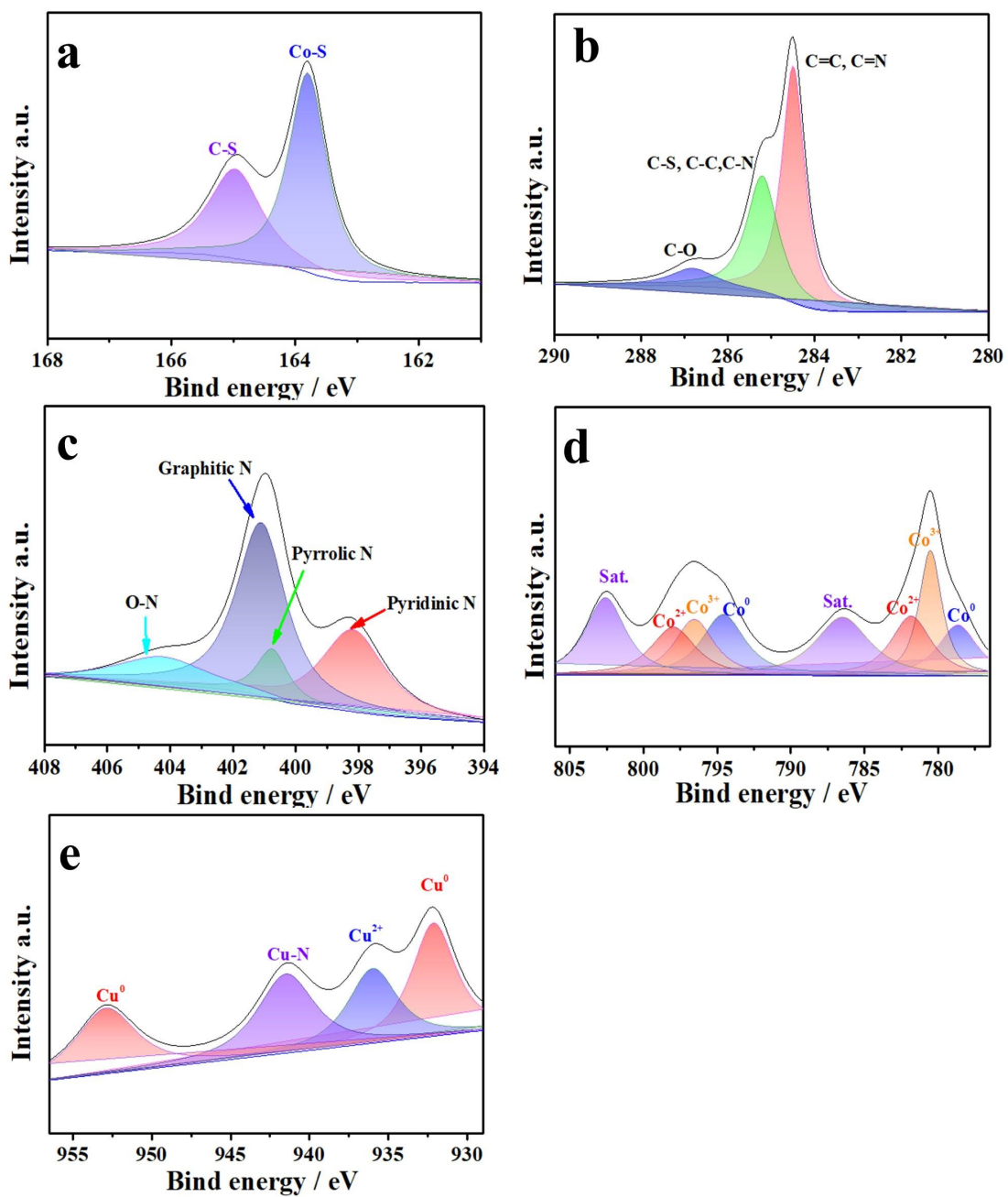


**Figure S12.** High-resolution S 1s (d), C 1s (a), N 1s (b), Co 2p (c), spectra of Cu/Co/CoS<sub>2</sub>@S,N-C (5 mg).

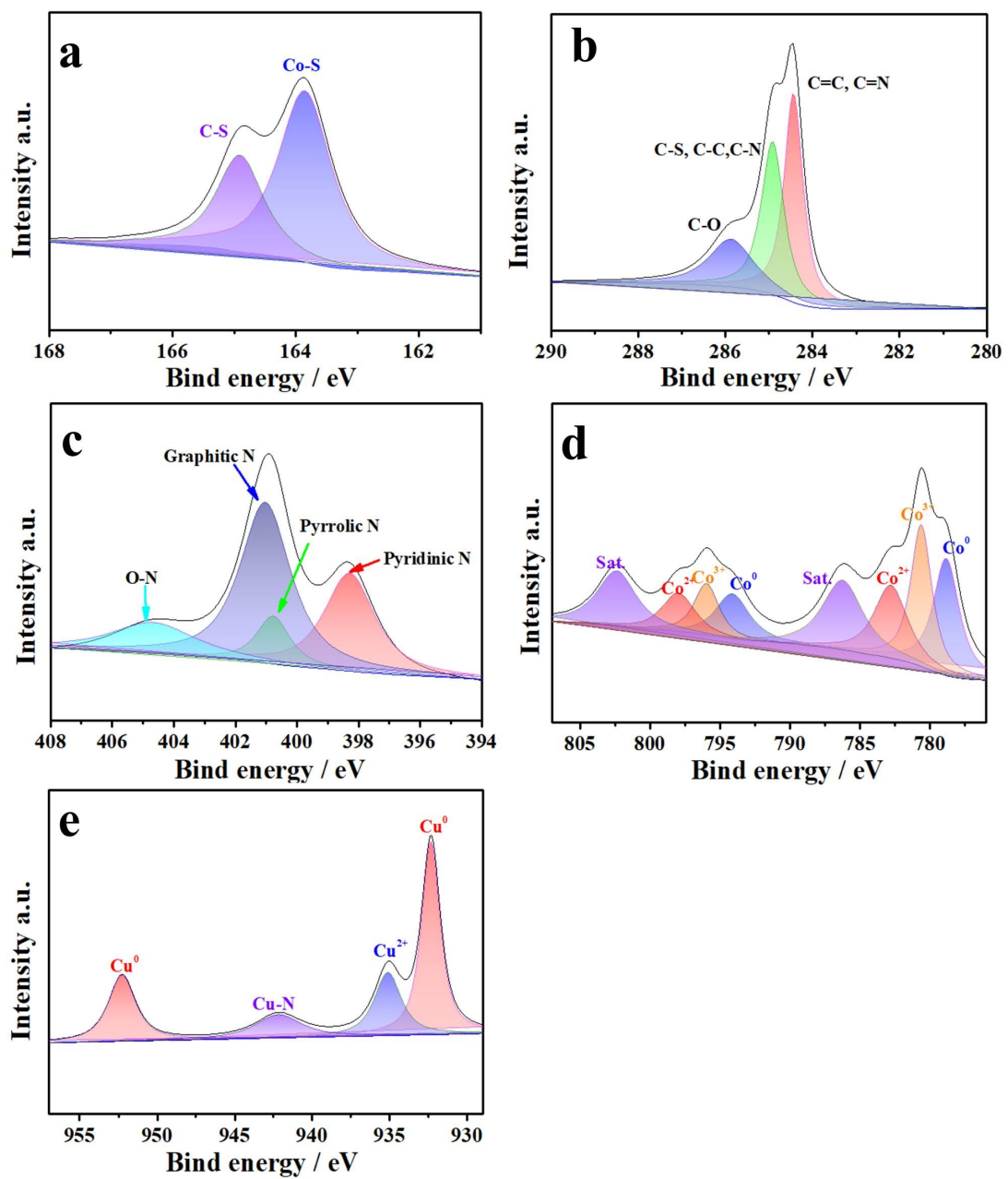


**Figure S13.** High-resolution S 1s (d), C 1s (a), N 1s (b), Co 2p (c), spectra of Cu/Co/CoS<sub>2</sub>@S,N-C (100 mg).

**Table S1** Pyridinic N & graphitic N dopant, sp<sup>2</sup>C content and the  $I_D/I_G$  value of Cu/Co/CoS<sub>2</sub>@S,N-C, Cu/Co/CoS<sub>2</sub>@S,N-C-900, Cu/Co/CoS<sub>2</sub>@S,N-C-1100, Cu/Co/CoS<sub>2</sub>@S,N-C (5 mg) and Cu/Co/CoS<sub>2</sub>@S,N-C (100 mg).

Sample	pyridinic N& graphitic N	sp <sup>2</sup> C	$I_D/I_G$
Cu/Co/CoS <sub>2</sub> @S,N-C	80 %	61 %	1.88
Cu/Co/CoS <sub>2</sub> @S,N-C-900	70 %	48 %	1.51
Cu/Co/CoS <sub>2</sub> @S,N-C-1100	67 %	51%	1.43
Cu/Co/CoS <sub>2</sub> @S,N-C (5 mg)	69 %	44%	1.41
Cu/Co/CoS <sub>2</sub> @S,N-C (100 mg)	72 %	55%	1.55

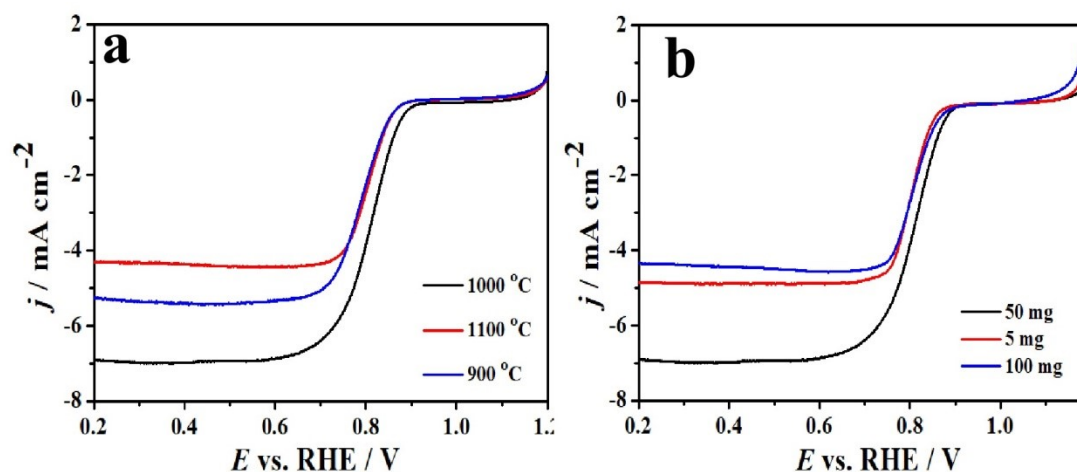


**Figure S14.** (a) LSV curves of the Cu/Co/CoS<sub>2</sub>@S,N-C made from Cu(OH)<sub>2</sub> NRs/Co(OH)<sub>2</sub> NSs with variable contents in 0.1 M KOH; (b) LSVs of the Cu(OH)<sub>2</sub> NRs/Co(OH)<sub>2</sub> NSs calcined at various temperatures.

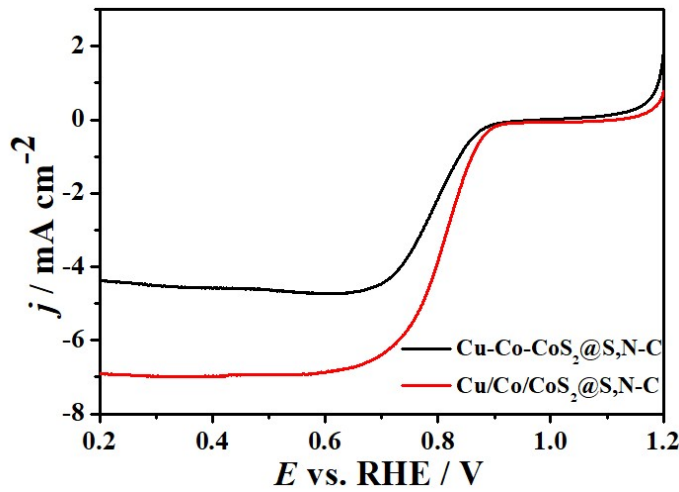


**Figure S15.** LSV curves of the Cu-Co-CoS<sub>2</sub>@S,N-C and Cu/Co/CoS<sub>2</sub>@S,N-C.

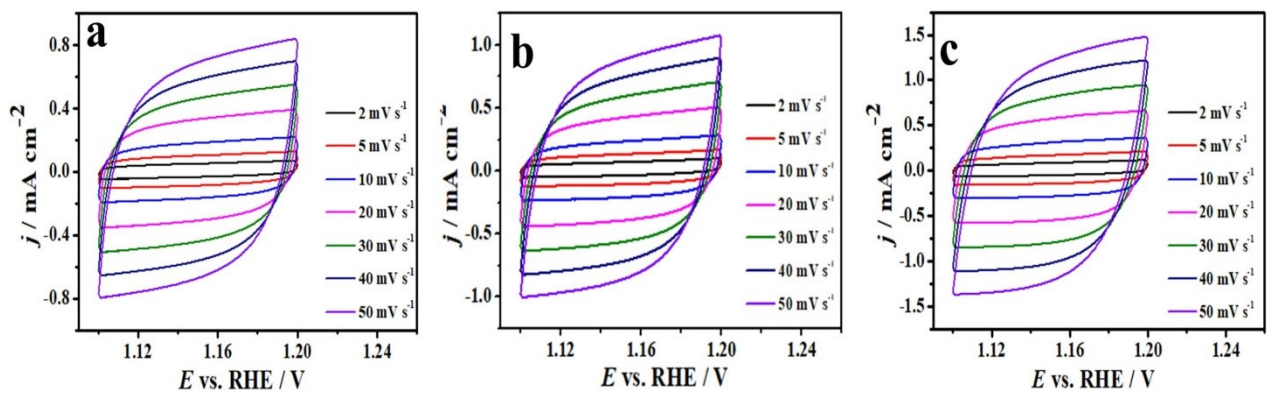


**Figure S16.** CV curves of the Co/CoS<sub>2</sub>@S,N-C, Cu/Co@NC and Cu/Co/CoS<sub>2</sub>@S,N-C.

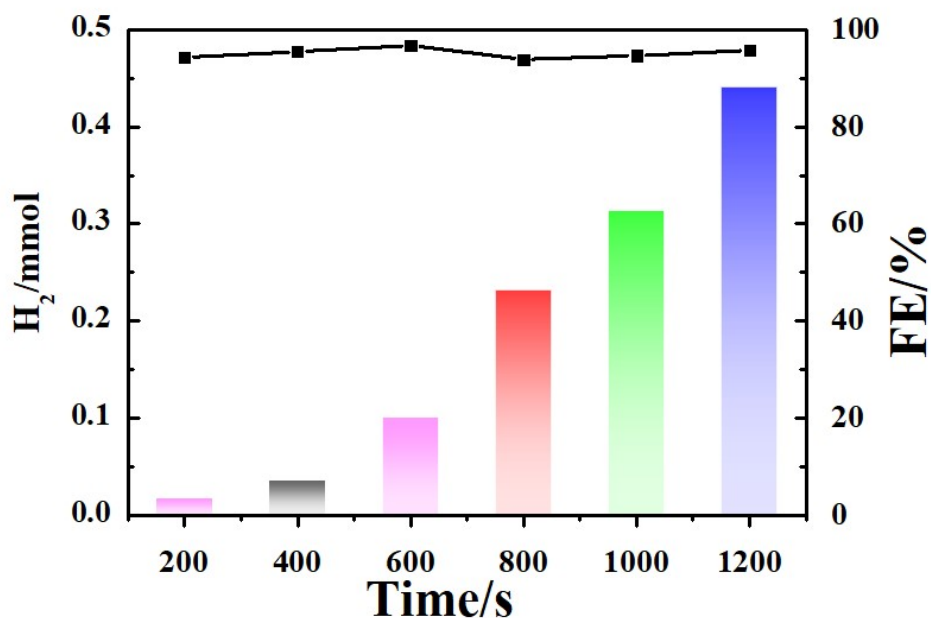


**Figure S17.** Gas volume versus time and corresponding Faradaic efficiency of Cu/Co/CoS<sub>2</sub>@S,N-C.

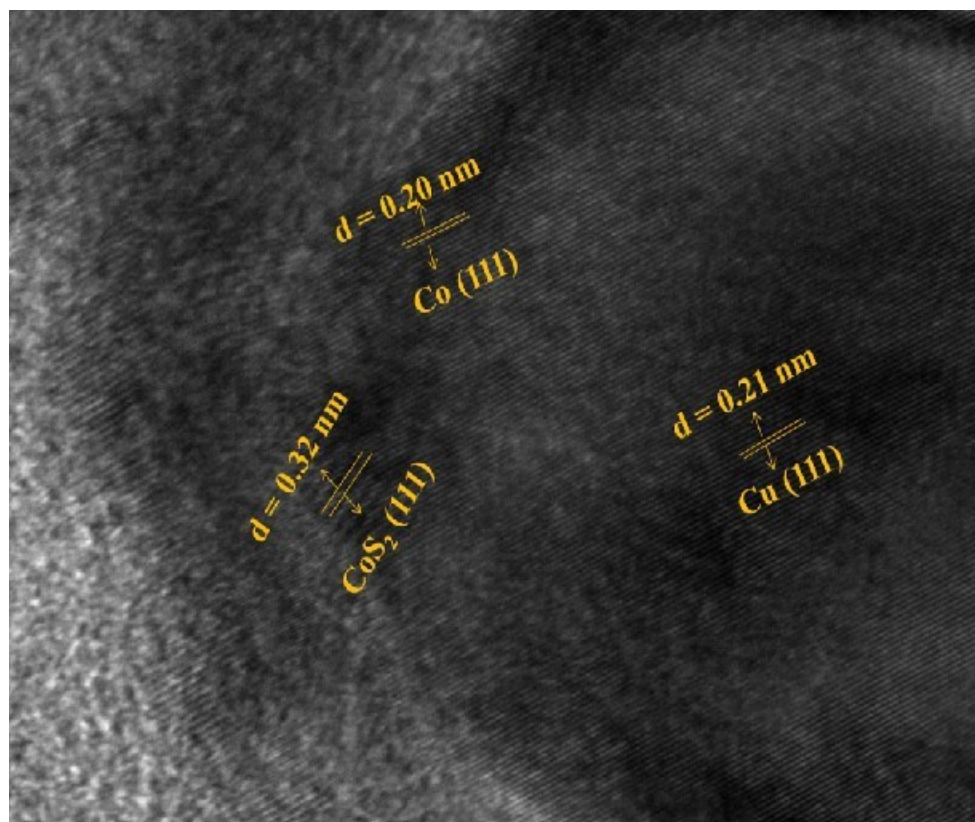


**Figure S18.** Magnified HRTEM image of Cu/Co/CoS<sub>2</sub>@S,N-C.

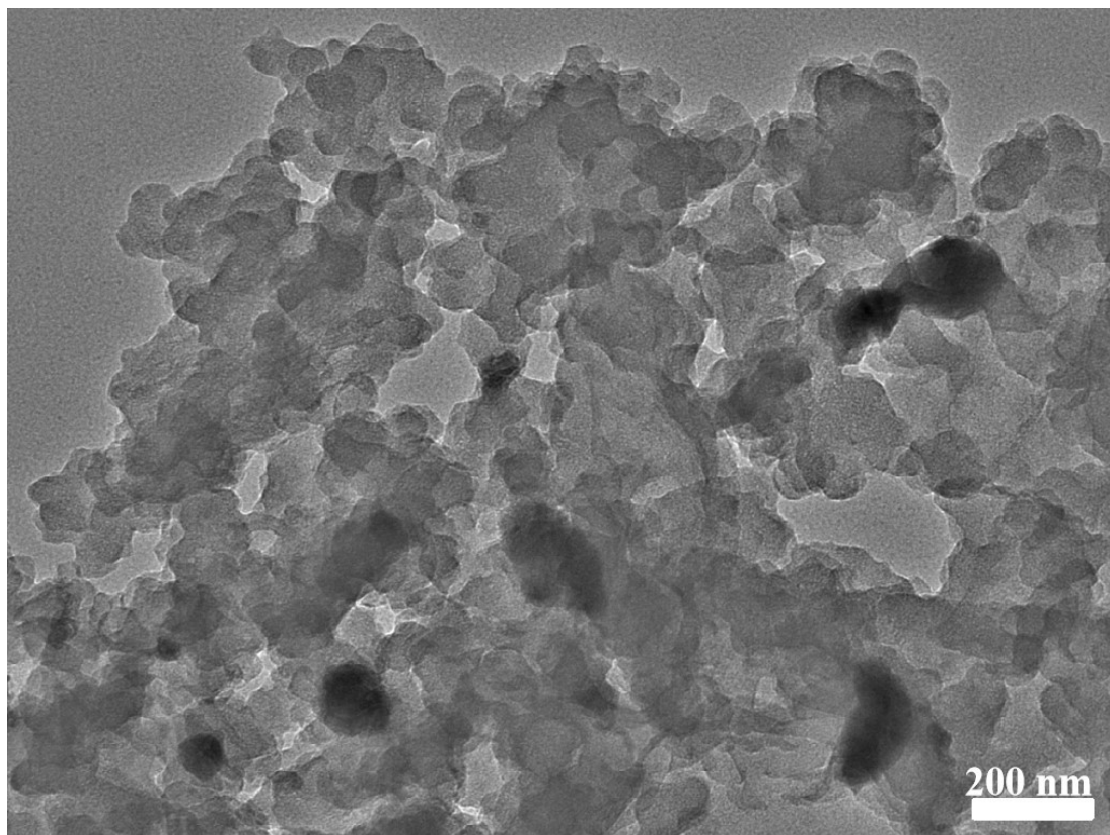


Figure S19. TEM image of Cu/Co/CoS<sub>2</sub>@S,N-C after 30000 s.

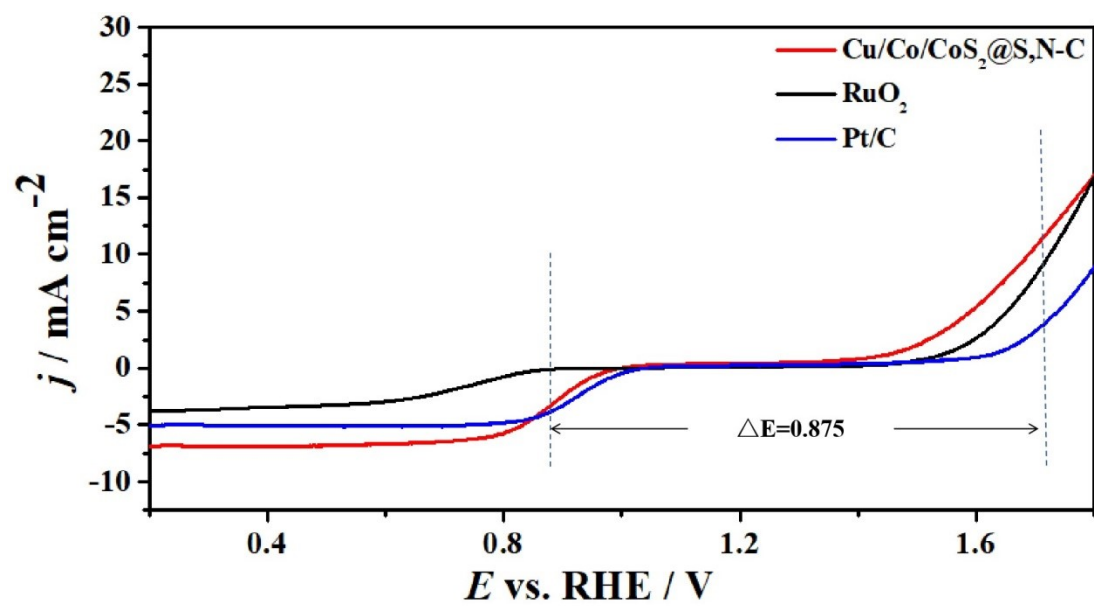


Figure S20. Bifunctional catalytic activity between the ORR and OER of Cu/Co/CoS<sub>2</sub>@S,N-C, RuO<sub>2</sub> and Pt/C.

**Table S2** Comparison of ORR/OER performances of reported Cu/Co/CoS<sub>2</sub>@S,N-C - based electrocatalysts.

Catalysts	$E_{\text{onset, ORR}} (\text{V})$	$E_{1/2,\text{ORR}} (\text{V})$	Current density ( $\text{mA cm}^{-2}$ )	Electrolyte	$E_{j=10, \text{OER}} (\text{V})$	Electrolyte	Reference
Cu/Co/CoS <sub>2</sub> @S,N-C	0.881	0.811	7.03	0.1 M	1.657	0.1 M	This work
M-NC-CoCu	0.85	0.75	-	0.1 M	1.54	1 M	<sup>1</sup>
CuCoS-4/N-rGO	0.97	0.86	5.2	0.1 M	1.52	1 M	<sup>2</sup>
CuCoS/CC	-	-	-	-	1.51	1 M	<sup>3</sup>
Cu-SAs@N-CNS	1.01	0.9	5.5	0.1 M	-	-	<sup>4</sup>
CaMnO <sub>3</sub> - $\delta$	0.84	0.80	4.27	0.1M	-	-	<sup>5</sup>
Co-S-C-700	0.8	0.79	-	0.1 M	1.58	0.1 M	<sup>6</sup>
CoNi/NHCS-TUC-3	0.91	0.88	5.13	0.1 M	-	-	<sup>7</sup>
Co <sub>0.5</sub> Fe <sub>0.5</sub> S@N-MC	0.913	0.808	5	0.1 M	1.57	1 M	<sup>8</sup>
Fe-Co-S/N	-	-	-	-	1.56	1 M	<sup>9</sup>
Zn-Co-S@NSC	0.955	-	5.92	0.1 M	-	-	<sup>10</sup>

## References

1. A. M. Andrade, Z. Liu, S. Grewal, A. J. Nelson and H. L. Min, MOF-derived Co/Cu-embedded N-doped carbon for trifunctional ORR/OER/HER catalysis in alkaline media, *Dalton Trans.*, 2021, **50**, 5473-5482.
2. H. Zhang, X. Wang, Z. Yang, S. Yan, C. Zhang and S. Liu, Space-confined synthesis of lasagna-like N-doped graphene-wrapped copper–cobalt sulfides as efficient and durable electrocatalysts for oxygen reduction and oxygen evolution reactions, *ACS Sustainable Chem. Eng.*, 2019, **8**, 1004-1014.
3. H. Luo, H. Lei, Y. Yuan, Y. Liang, Y. Qiu, Z. Zhu and Z. Wang, Engineering ternary copper-cobalt sulfide nanosheets as high-performance electrocatalysts toward oxygen evolution reaction, *Catalysts*, 2019, **9**, 459.
4. L. Zong, K. Fan, W. Wu, L. Cui, L. Zhang, B. Johannessen, D. Qi, H. Yin, Y. Wang, P. Liu, L. Wang and H. Zhao, Anchoring single copper atoms to microporous carbon spheres as high - performance electrocatalyst for oxygen reduction reaction, *Adv. Funct. Mater.*, 2021, **31**, 2104864.

5. N. Tham, X. Ge, A. Yu, B. Li, Y. Zong and Z. Liu, Porous calcium–manganese oxide/carbon nanotube microspheres as efficient oxygen reduction catalysts for rechargeable zinc–air batteries, *Inorg. Chem. Front.*, 2021, **8**, 368-375.
6. J. Tan, R. Li, S. A. Raheem, L. Pan, H. Shen, J. Liu, M. Gao and M. Yang, Facile construction of carbon encapsulated of earth - abundant metal sulfides for oxygen electrocatalysis, *ChemElectroChem*, 2021, **8**, 3533-3537.
7. K. Sheng, Q. Yi, A. L. Chen, Y. Wang, Y. Yan, H. Nie and X. Zhou, CoNi nanoparticles supported on N-doped bifunctional hollow carbon composites as high-performance ORR/OER catalysts for rechargeable Zn-air batteries, *ACS Appl. Mater. Interfaces*, 2021, **13**, 45394-45405.
8. M. Shen, C. Ruan, Y. Chen, C. Jiang, K. Ai and L. Lu, Covalent entrapment of cobalt–iron sulfides in N-doped mesoporous carbon: extraordinary bifunctional electrocatalysts for oxygen reduction and evolution reactions, *ACS Appl. Mater. Interfaces*, 2015, **7**, 1207-1218.
9. X. Li, G. Zhu, L. Xiao, Y. Liu, Z. Ji, X. Shen, L. Kong and S. A. Shah, Loading of Ag on Fe-Co-S/N-doped carbon nanocomposite to achieve improved electrocatalytic activity for oxygen evolution reaction, *J. Alloys Compd.*, 2019, **773**, 40-49.
10. C. Li, J. Balamurugan, N. H. Kim and J. H. Lee, Hierarchical Zn-Co-S nanowires as advanced electrodes for all solid state asymmetric supercapacitors, *Adv. Energy Mater.*, 2018, **8**, 1702014.